Atomically precise graphene nanoribbon heterojunctions from a single molecular precursor

Giang D. Nguyen[1‖‡], Hsin-Zon Tsai[1‡], Arash A. Omrani[1‡], Tomas Marangoni[2‡], Meng Wu[1‡], Daniel J. Rizzo[1], Griffin F. Rodgers[1], Ryan R. Cloke[2], Rebecca A. Durr[2], Yuki Sakai[5], Franklin Liou[1], Andrew S. Aikawa[1], James R. Chelikowsky[5], Steven G. Louie[1,3,4,*], Felix R. Fischer[2,3,4,*] and Michael F. Crommie[1,3,5,*]

[1] Department of Physics, University of California at Berkeley, Berkeley, CA 94720, USA.

[2] Department of Chemistry, University of California at Berkeley, Berkeley, CA 94720, USA.

[3] Materials Sciences Division, Lawrence Berkeley National Laboratory, Berkeley, CA 94720, USA.

[4] Kavli Energy NanoSciences Institute at the University of California Berkeley and the Lawrence Berkeley National Laboratory, Berkeley, CA 94720, USA.

[5] Center for Computational Materials, Institute for Computational Engineering and Sciences, Departments of Physics and Chemical Engineering, The University of Texas at Austin, Austin, Texas 78712, USA

‖ Present address: Center for Nanophase Materials Sciences, Oak Ridge National Laboratory, Oak Ridge, Tennessee 37831, USA

‡ These authors contributed equally

Abstract

The rational bottom-up synthesis of atomically defined graphene nanoribbon (GNR) heterojunctions represents a key enabling technology for the design of nanoscale electronic devices. Synthetic strategies have thus far relied on the random copolymerization of two electronically distinctive molecular precursors to yield a segmented band structure within a GNR. Here we report the fabrication and electronic characterization of atomically precise GNR heterojunctions prepared through a late-stage functionalization of chevron GNRs obtained from a single precursor that features fluorenone substituents along the convex edges. Excitation of the GNR induces cleavage of sacrificial carbonyl groups at the GNR edge, thus giving rise to atomically well-defined heterojunctions comprised of segments of fluorenone GNR and unfunctionalized chevron GNR. The structure of fluorenone/unfunctionalized GNR heterojunctions was characterized using bond-resolved STM (BRSTM) which enables chemical bonds to be imaged via STM at T = 4.5 K. Scanning tunneling spectroscopy (STS) reveals that the band alignment across the interface yields a staggered gap Type II heterojunction and is consistent with first-principles calculations. Detailed spectroscopic and theoretical studies reveal that the band realignment at the interface between fluorenone and unfunctionalized chevron GNRs proceeds over a distance less than 1nm, leading to extremely large effective fields.

Introduction

The tunable electronic structure of graphene nanoribbons (GNRs) has attracted great interest due to potential applications in synthetic electronic devices.[1–4] Although several top-down techniques exist for fabricating GNRs, only bottom-up synthesis of GNRs from molecular

precursors yields nanoribbons with atomically-defined structure and dopant control.[5–10] A unique aspect of bottom-up GNRs is that they provide extensive opportunities for creating atomically precise molecular heterojunctions where two different GNR types bond at an interface. Predictions have been made that such heterojunctions will play a useful role in future nanotechnologies, including fabrication of robust molecular diodes and transistors.[11,12] While the behavior of heterojunctions in macroscopic semiconductor crystals has been extensively studied,[13] heterojunction behavior in molecular nanostructures is not as well understood.[14–17] Bottom-up GNR heterojunctions have previously been fabricated by an approach that combines two different molecular precursor types, thus yielding either impurity-modulated[18] or width-modulated[19] GNR heterojunctions. This fabrication method, however, depends on the random process of precursor self-assembly and does not allow heterojunction fabrication or modification after a GNR has been synthesized.

In this work we report a new technique for fabricating bottom-up GNR heterojunctions through post-growth manipulation that results in atomically perfect heterojunction structures from a single precursor. Such post-growth modification of GNR electronic properties offers a more flexible route for heterojunction fabrication, thus enabling additional bottom-up control that could lead to more complex future molecular device architectures. Single-precursor-based heterojunctions were achieved through the design and implementation of a new type of GNR precursor molecule that incorporates sacrificial carbonyl groups and results in carbonyl-decorated fluorenone GNRs (Fig. 1a). While the carbonyl groups survive the GNR synthesis process, they can be removed later by exciting the fluorenone GNR (e.g., temperature, electric field). Fluorenone GNRs are found to have a different band gap and energy alignment than unfunctionalized chevron GNRs, thus enabling fabrication of Type II heterojunctions between

carbonyl-decorated and carbonyl-free GNR segments that exhibit atomically precise interfaces. Type II heterojunction behavior in partially decarbonylated fluorenone GNRs was experimentally confirmed via a bond-resolved STM imaging technique (BRSTM) that allows determination of local chemical structure in combination with scanning tunneling spectroscopy (STS) to unambiguously characterize the local band alignment profile of the heterojunction. We observe that the electronic structure of atomically-precise bottom-up GNR heterojunctions can fully transition between different band gaps over a length scale of less than 1 nm across a heterojunction interface. The interpretation of our experimental data is strongly supported by first-principles calculations.

Discussion

Chevron-type graphene nanoribbons (GNRs) featuring a regular pattern of 9*H*-fluoren-9-one substituents along their convex edges were prepared from molecular precursor **1** through a sequential radical step-growth polymerization/cyclodehydrogenation procedure on a Au(111) surface (Fig. 1a).[3,5,8,10,20] Fig. 1b shows a representative STM topographic image of a GNR functionalized with fluorenone substituents recorded with a CO-functionalized tip. The distinctive carbonyl group introduced with the fluorenone substituent is not resolved in routine STM images, thus fluorenone GNRs appear indistinguishable from unfunctionalized chevron-type GNRs.[3,18] In order to resolve the carbonyl group and verify the chemical structure of fluorenone GNRs, we developed a new bond-resolved STM imaging technique (BRSTM) which is an extension of techniques described in recently published work.[21] This technique provides bond-resolved contrast of molecular nanostructures without employing the additional complexity of noncontact atomic force microscopy (nc-AFM) or the need to operate at sub-Kelvin temperatures.[22,25] The contrast in BRSTM images relies on changes in the differential

conductivity (dI/dV) of the STM tunneling junction at low bias (20–50 mV) measured with a CO-functionalized STM tip (see Methods).[21] BRSTM imaging of fluorenone functionalized GNRs (Fig. 1c) clearly resolves the distinctive structure of the chevron-type GNR backbone as well as the cyclopentadienone groups derived from the fluorenone substituents in **1**. The fluorenone oxygen atoms appear as bright spots protruding from the apex of the convex GNR edges. This structural assignment was independently confirmed using well established CO-tip-functionalized nc-AFM imaging[22,23] and simulation techniques[21] (Supplementary Information Figs. S2,7).

The local electronic structure of fluorenone GNRs on Au(111) was characterized by STS using a CO-functionalized tip. Fig. 2a shows a characteristic dI/dV point spectrum recorded at a position above the cyclopentadienone of a uniform fluorenone GNR (red curve). The dI/dV spectrum of an unfunctionalized chevron GNR prepared independently from a suitable precursor is also shown as a reference (blue curve). The dI/dV spectrum of fluorenone GNRs shows peaks at +1.37 ± 0.03 eV and −0.96 ± 0.01 eV relative to the Fermi energy (V = 0). The peak at −0.96 eV is identified as the fluorenone GNR valence band (VB) edge while the peak at +1.37 eV is identified as the conduction band (CB) edge. The resulting band gap for a fluorenone GNR is 2.33 ± 0.03 eV. The corresponding band edge features for unfunctionalized chevron GNRs yield a VB edge of −0.83 ±0.03 eV, a CB edge of 1.70 ±0.04 eV, and a band gap of 2.53 ± 0.05 eV (Fig. S3) (careful control of our STM tips and good statistics have allowed us to reduce the unfunctionalized chevron band gap uncertainty compared to earlier publications[6,18]). The introduction of a fluorenone substituent thus leads to a shift of the GNR band edges to lower energies and an overall reduction of the band gap by 0.20 ± 0.06 eV.

The spatial distribution of the fluorenone GNR local density of states (LDOS) at energies close to the CB and VB edges was experimentally determined using constant current dI/dV mapping (Figs. 2c,e). At an imaging bias of –1.0 V the LDOS associated with the VB edge is strongest along the concave edges of the fluorenone GNR (Fig. 2c) while the intensity decreases at the convex edges coinciding with the position of the fluorenone group. An LDOS map near the CB edge recorded at +1.35 V (Fig. 2e) shows distinctly stronger intensity near the fluorenone group. dI/dV maps acquired for unfunctionalized chevron GNRs (see SI Fig. S3) similarly show highest LDOS along the GNR edges. A prominent difference between the unfunctionalized chevron GNR dI/dV maps and the fluorenone GNR dI/dV maps is that the presence of carbonyl groups at the convex edges of the ribbon induces a node in the LDOS intensity that is not observed for unfunctionalized chevron GNRs (see SI Fig. S3).

Bottom-up GNR heterojunctions were prepared by cleaving all carbonyl groups within localized segments of fluorenone GNRs by thermal annealing (STM tip-induced site-specific decarbonylation was also observed (see SI)). A heterojunction in this context corresponds to a segment of decarbonylated chevron GNR (i.e., unfunctionalized chevron GNR) and a segment of fluorenone GNR that are covalently linked by an atomically defined interface (Fig. 3a) (we have not observed any significant dependence of heterojunction properties on the length of the various GNR segments). Fig. 3b shows a BRSTM image of a GNR heterojunction formed in this way by annealing a uniform fluorenone GNR at 350 °C in UHV for 1 hr. An example of tip-induced cleaving is shown in Fig. S5.

STS reveals that the local electronic structure at the interface of a bottom-up synthesized fluorenone/unfunctionalized heterojunction yields a Type II staggered gap heterojunction. This can be seen in Fig. 3c which shows dI/dV point spectra recorded at positions on opposite sides of

the heterojunction interface (the respective positions are highlighted in Fig. 3b). The band edges of the fluorenone GNR segment are shifted to lower energy with respect to the unfunctionalized chevron GNR segment (this behavior did not significantly depend on the GNR orientation with respect to the underlying gold surface). Such spatial separation of heterojunction states at the CB edge (peak 1) and VB edge (peak 2) across an interface is the hallmark of Type II heterojunctions.[13,24]

In an effort to better understand the evolution of the heterojunction electronic structure across the junction interface, we acquired dI/dV point spectra along the GNR edge on either side of a heterojunction interface (see tip trajectory sketch in Fig. 4a). The spatial dependence of the experimental spectra (Fig. 4b) shows the change in band edge energies as the STM tip moves across the interface (dashed white line). This band bending (~0.3 eV in the conduction band) occurs over a distance of only 0.6 nm, leading to extremely large effective fields in the conduction band on the order of 5×10^8 V m^{-1} across the GNR heterojunction interface. Such fields were theoretically predicted in a previous study of GNR heterojunctions.[18]

We used dI/dV mapping to resolve the LDOS patterns associated with VB and CB wave functions at the heterojunction interface. Fig. 5 shows a BRSTM topographic image of a GNR featuring a central unfunctionalized chevron GNR segment with fluorenone GNR segments fused on either side. The positions of carbonyl groups in the fluorenone GNR segments are clearly resolved (red arrows), thus allowing precise determination of heterojunction interface locations. Fig. 5b shows a dI/dV map of this GNR recorded at an imaging bias of +1.35 V that corresponds to the CB edge (peak 1) seen in Fig. 3c. The LDOS of the CB state is clearly localized to the fluorenone segments and shows the characteristic pattern associated with the CB edge of uniform fluorenone GNRs (Fig. 2e). A dI/dV map of the same region obtained at an

imaging bias of –0.83 V corresponding to the VB edge (peak 2) in Fig. 3c shows very different behavior. Here the LDOS has highest intensity in the central unfunctionalized GNR segment, while the fluorenone segments remain dark (Fig. 5c). The heterojunction CB edge and VB edge states are directly observed to separately localize to the fluorenone and unfunctionalized GNR segments, respectively.

Our experimental results are consistent with theoretical simulations based on *ab initio* calculations, thus providing strong evidence that the effects observed here are intrinsic features of atomically precise GNR heterojunctions. We first simulated the behavior of uniform fluorenone and unfunctionalized chevron GNRs separately using density functional theory (DFT) at the LDA level. The theoretical density of states (DOS) of fluorenone and unfunctionalized chevron GNRs are plotted in Fig. 2b. The predicted band gap of a fluorenone GNR is 0.21 eV smaller than the bandgap of an unfunctionalized GNR, and the fluorenone VB and CB edges are shifted to lower energy (calculated band structures are shown in the Supplementary Information Fig. S4). While the magnitude of the theoretical band gaps and band edge shifts cannot be quantitatively compared to the experimental data (LDA calculations are known to underestimate energy gaps) the experimentally observed trends are reproduced by the calculations. The reduced band gap and band edge shifts observed for fluorenone GNRs can be intuitively understood as the result of an extension of the GNR π-network (and thus weaker quantum confinement) to include the fluorenone group and the electron withdrawing effect of the carbonyl groups at the convex edges respectively.

A direct comparison between experimental dI/dV maps and theoretical LDOS plots shows good agreement for states at the GNR band edges. Fig. 2d shows the calculated LDOS map of states at the VB edge for a uniform fluorenone GNR. The highest intensity is seen to be

localized along the concave edges of the GNR, consistent with the experimental VB d*I*/d*V* map depicted in Fig. 2c. Similarly, the characteristic pattern reflected in the theoretical LDOS of states at the fluorenone CB edge (Fig. 2f) is in good agreement with the experimental CB d*I*/d*V* map depicted in Fig. 2e. (Theoretical LDOS maps for unfunctionalized chevron GNRs are similarly consistent with experimental d*I*/d*V* maps, see SI Fig. S3).

In an effort to better understand the intrinsic band alignment of a fluorenone/unfunctionalized GNR heterojunction we calculated the electronic structure of the bond-resolved experimental heterojunction system depicted in Fig. 5a. The unit cell used in the calculation (Fig. 5e) comprises a central unfunctionalized chevron GNR segment flanked on both sides by short segments of fluorenone GNRs, precisely as seen experimentally in Fig. 5a. A plot of the calculated energy-dependent LDOS at points along the edge of the heterojunction in Fig. 5d (black dashed line) is depicted in Fig 4c. The theoretical band gap is smaller in the fluorenone segment (left side of the heterojunction) than in the unfunctionalized chevron segment (right side of the heterojunction) and is consistent with the experimental data in Fig. 4b. Both the theoretical and experimental band structure realignment across the heterojunction interface are remarkably similar and occur over a distance of less than 1 nm. This confirms previous predictions[18] that atomically precise GNR heterojunctions should induce extremely large effective electric fields.

The unusually sharp transition of the band edge states across the heterojunction interface is further supported by the high degree of localization observed in the theoretical heterojunction LDOS at energies close to the band edges. At the CB edge the theoretical LDOS of the heterojunction structure shown in Fig. 5d is largely localized to the fluorenone substituted segments (Fig. 5e). The LDOS pattern here exhibits the same recurring motif calculated for the CB LDOS of uniform fluorenone GNRs (Fig. 2f), and closely resembles the experimental CB

LDOS pattern of the heterojunction displayed in Fig. 5b. At energies close to the VB edge the theoretical LDOS alternatively shows localization to the unfunctionalized chevron GNR segment (Fig. 5f). The characteristic VB pattern is the same as the LDOS pattern calculated for uniform unfunctionalized GNRs (Supplementary Information Fig. S3c) and matches the spatial localization observed experimentally in the dI/dV image of Fig. 5c. Agreement between experimental and theoretical data for the CB and VB edges of the heterojunction confirm wavefunction localization consistent with a Type II heterojunction and also indicate that substrate interaction effects do not play a significant role in determining the wavefunction symmetry or spectroscopic peak ordering for this GNR system. However, it should be noted that DFT-LDA calculations are known to underestimate absolute bandgap magnitude for low-dimensional semiconductor systems[28] and that substrate screening can also lead to bandgap renormalization.[19]

In conclusion, we have demonstrated rational fabrication of bottom-up synthesized GNR Type II heterojunctions using only a single precursor type via post-synthesis cleaving of carbonyl groups. We have developed a bond-resolved STM imaging technique (BRSTM) that allows us to observe the atomically defined structure of GNR heterojunctions, enabling highly resolved structure/function characterization without the need for nc-AFM[22] or ultra-low temperature[25] measurement. Our STS measurements reveal that the CB and VB states of the heterojunction are strongly localized to the fluorenone and unfunctionalized segments respectively of the GNR, consistent with Type II heterojunction behavior. Theoretical simulations based on ab initio DFT calculations confirm this interpretation, including the generation of effective field strengths as high as 5×10^8 Vm^{-1} within the conduction band of atomically precise heterojunction interfaces. This work suggests a new strategy for implementing

bond-targeted post-processing GNR modifications to create more complex molecular heterostructures via bottom-up synthesis for future molecular electronics and memory applications.

Methods

Molecular synthesis

The molecular precursor for fluorenone GNRs **1** was prepared via Sonogashira-Hagihara cross-coupling of 4-bromo-9*H*-fluoren-9-one with ethynyltrimethylsilane. Deprotection of the TMS group yields 4-ethynyl-9*H*-fluoren-9-one in. Diels-Alder cycloaddition of 4-ethynyl-9*H*-fluoren-9-one with 5,10-dibromo-1,3-diphenyl-2H-cyclopenta[*l*]phenanthren-2-one followed by cheletropic extrusion of CO affords the GNR precursor **1**. Detailed experimental procedures and characterization can be found in the Supplementary Information.

Experimental methods

GNRs and GNR heterojunctions were fabricated on a Au(111) thin film substrate. Standard Ar^+ sputtering and annealing cycles were used to prepare a clean surface. The molecular precursor **1** was deposited at 420 K from a home-built Knudsen cell evaporator onto the Au(111) substrate held at 298 K under ultra-high vacuum for ~5 min to obtain 30–70% monolayer coverage. After deposition the surface was slowly annealed to 473 K for 30 min to induce dehalogenation and polymerization. The temperature was then increased slowly up to 573 K for 20 min to induce cyclodehydrogenation, thus yielding fluorenone GNRs. Heterojunctions composed of adjacent fluorenone and unfunctionalized chevron segments were obtained by thermally annealing the sample at 623 K for 1 hr to cleave CO groups from the GNR edges. Tip-based removal of carbonyl groups was performed by placing the STM tip over a single carbonyl group with tunnel

parameters V_s = 3 V and I = 10 pA and then ramping the current up to 500 pA over 30 sec. The unfunctionalized chevron GNR is prepared using the same molecular precursor as in ref. 3. The GNR is synthesized by annealing at 473 K to form polymers and at 673 K to form GNRs. All SPM experiments were performed using a commercial Omicron LT-STM at 4.5 K. W tips with and without CO functionalization were used for STM and STS measurement. *dI/dV* spectra showed no appreciable difference in the peak positions between bare W-tips and those functionalized with a CO molecule. CO-functionalized tips generally provided better resolution in both topographic images and d*I*/d*V* maps. d*I*/d*V* measurements were recorded using a lock-in amplifier with modulation frequency and voltage of 401 Hz and 6–10 mV_{rms}, respectively. *dI/dV* point spectra were recorded under open feedback loop conditions while *dI/dV* maps were recorded under constant current conditions (constant height *dI/dV* maps yielded similar results to constant current *dI/dV* maps). Bond-resolved STM (BRSTM) imaging was accomplished by first functionalizing the STM tip with a CO molecule. The surface was then scanned in constant current mode at low DC bias (20–50 mV) with an AC wiggle voltage added to the tip (modulation frequency and voltage of 401 Hz, 20 mV_{rms}) while recording the out-of-phase d*I*/d*V* signal (the out-of-phase signal here does not come from capacitive coupling but rather from tip oscillation driven by the feedback loop). The BRSTM images shown in Figs. 1, 3, and 5 show the out-of-phase d*I*/d*V* signal. More than 5 heterojunctions were characterized via STS using numerous different STM tips.

Theoretical calculation

First-principles calculations for fluorenone GNRs, unfunctionalized chevron GNRs, and fluorenone/unfunctionalized GNR heterojunctions were performed using DFT at the LDA level, as implemented in the Quantum Espresso package[26]. Only free-standing GNRs were simulated

(i.e., no substrate was included). We used norm-conserving pseudopotentials[27] with a plane wave kinetic energy cut-off of 80 Ry. For the heterojunction calculations we constructed a periodic superlattice structure in which each unit cell was identical to the measured experimental heterojunction structure. This structure was fully relaxed until the force on each atom was smaller than 0.05 eV$\cdot$ Å^{-1}. Dangling bonds on the edges were all passivated by hydrogen atoms. LDOS calculations were performed at 4 Å above the atomic plane. The spatial- and energy-resolved LDOS across the fluorenone/unfunctionalized heterojunction was calculated by scanning the energy range with a step of 0.02 eV, and averaging the LDOS contribution within a circle of 4 Å radius along the path (0.1 eV Gaussian broadening was applied here). It should be pointed out that although DFT-LDA calculations are known to underestimate the quasiparticle energy gap in low-dimensional systems, such as graphene nanoribbons,[28] the description of quasiparticle wavefunctions at LDA level is justified by our previous work.[19] Also we did not include substrate screening in our calculations, which might introduce noticeable reduction of quasiparticle bandgaps compared with suspended samples. However, these factors are not expected to alter the peak ordering assignments, as discussed in our previous work.[19]

ACKNOWLEDGMENTS

Research supported by the Office of Naval Research BRC Program (spectroscopic imaging), by the U.S. Department of Energy (DOE), Office of Science, Basic Energy Sciences (BES), under award no. DE-SC0010409 (design, synthesis, and characterization of molecular precursors) and Nanomachine Program award no. DE-AC02-05CH11231 (surface reaction characterization and band structure calculations), by DARPA, the U. S. Army Research Laboratory and the U. S. Army Research Office under contract/grant number W911NF-15-1-0237 (tip-based manipulation), and DMR-1508412 (development of theory formalism and STM analyses).

Computational resources have been provided by the DOE at Lawrence Berkeley National Laboratory's NERSC facility and by the NSF through XSEDE resources at NICS. YS and JRC wish to acknowledge support by the U.S. Department of Energy under Contract DOE/DE-FG02-06ER46286 (AFM simulation) and the Welch Foundation under Grant F-1837 (image analysis).

Author contributions

T.M., R.R.C., R.A.D. and F.R.F. designed, synthesized, and characterized the molecular precursors. G.D.N., H.T., A.A.O., D.J.R., G.F.R., F.L. and A.S.A. performed STM and nc-AFM measurements. G.D.N., H.T., A.A.O. and D.J.R. performed data analysis. M.W. and S.G.L. performed DFT calculations and interpretation of STM data. Y.S. and J.R.C. performed theoretical simulation for BRSTM imaging. M.F.C. supervised the experimental scanned probe measurements and helped to interpret the results. All authors contributed to the scientific discussion and helped in writing the manuscript.

Additional information

Supplementary information accompanies this paper at www.nature.com/naturenanotechnology.

Correspondence and requests for materials should be addressed to S.G.L. (sglouie@berkeley.edu), F.R.F. (ffischer@berkeley.edu), and M.F.C. (crommie@berkeley.edu).

Competing financial interests

The authors declare no competing financial interests.

References

1. Son, Y.-W., Cohen, M. L. & Louie, S. G. Half-metallic graphene nanoribbons. *Nature*

444, 347–349 (2006).

2. Shen, Y. T. *et al.* Switchable ternary nanoporous supramolecular network on photo-regulation. *Nano Lett.* **11,** 3245–3250 (2011).

3. Cai, J. *et al.* Atomically precise bottom-up fabrication of graphene nanoribbons. *Nature* **466,** 470–3 (2010).

4. Bennett, P. B. *et al.* Bottom-up graphene nanoribbon field-effect transistors. *Appl. Phys. Lett.* **103,** 253114 (2013).

5. Chen, Y. C. *et al.* Tuning the band gap of graphene nanoribbons synthesized from molecular precursors. *ACS Nano* **7,** 6123–6128 (2013).

6. Bronner, C. *et al.* Aligning the band gap of graphene nanoribbons by monomer doping. *Angew. Chemie - Int. Ed.* **52,** 4422–4425 (2013).

7. Nguyen, G. D. *et al.* Bottom-Up Synthesis of N = 13 Sulfur-Doped Graphene Nanoribbons. *J. Phys. Chem. C* **120,** 2684–2687 (2016).

8. Cloke, R. R. *et al.* Site-Specific Substitutional Boron Doping of Semiconducting Armchair Graphene Nanoribbons. *J. Am. Chem. Soc.* **137,** 8872–5 (2015).

9. Kawai, S. *et al.* Atomically controlled substitutional boron-doping of graphene nanoribbons. *Nat. Commun.* **6,** 8098 (2015).

10. Marangoni, T., Haberer, D., Rizzo, D. J., Cloke, R. R. & Fischer, F. R. Heterostructures through Divergent Edge Reconstruction in Nitrogen-Doped Segmented Graphene Nanoribbons. *Chem. - A Eur. J.* **22,** 13037–13040 (2016).

11. Yoon, Y. & Salahuddin, S. Barrier-free tunneling in a carbon heterojunction transistor.

Appl. Phys. Lett. **97,** 33102 (2010).

12. Ghoreishi, S. S., Saghafi, K., Yousefi, R. & Moravvej-Farshi, M. K. Graphene nanoribbon tunnel field effect transistor with lightly doped drain: Numerical simulations. *Superlattices Microstruct.* **75,** 245–256 (2014).

13. Neamen, D. A. *Semiconductor Physics and Devices: Basic Principles*. (McGraw-Hill, 2003).

14. Joachim, C., Gimzewski, J. K. & Aviram, A. Electronics using hybrid-molecular and mono-molecular devices. *Nature* **408,** 541–8 (2000).

15. Imada, H. *et al.* Real-space investigation of energy transfer in heterogeneous molecular dimers. *Nature* (2016). doi:10.1038/nature19765

16. Tao, C. *et al.* Spatial resolution of a type II heterojunction in a single bipolar molecule. *Nano Lett.* **9,** 3963–7 (2009).

17. Smerdon, J. A., Giebink, N. C., Guisinger, N. P., Darancet, P. & Guest, J. R. Large Spatially Resolved Rectification in a Donor–Acceptor Molecular Heterojunction. *Nano Lett.* **16,** 2603–2607 (2016).

18. Cai, J. *et al.* Graphene nanoribbon heterojunctions. *Nat. Nanotechnol.* **9,** 896–900 (2014).

19. Chen, Y.-C. *et al.* Molecular bandgap engineering of bottom-up synthesized graphene nanoribbon heterojunctions. *Nat. Nanotechnol.* **10,** 156–160 (2015).

20. Vo, T. H. *et al.* Nitrogen-Doping Induced Self-Assembly of Graphene Nanoribbon-Based Two-Dimensional and Three-Dimensional Metamaterials. *Nano Lett.* **15,** 5770–7 (2015).

21. Hapala, P. *et al.* Mechanism of high-resolution STM/AFM imaging with functionalized

tips. *Phys. Rev. B* **90,** 85421 (2014).

22. Gross, L., Mohn, F., Moll, N., Liljeroth, P. & Meyer, G. The chemical structure of a molecule resolved by atomic force microscopy. *Science* **325,** 1110–4 (2009).

23. de Oteyza, D. G. *et al.* Direct imaging of covalent bond structure in single-molecule chemical reactions. *Science* **340,** 1434–7 (2013).

24. Kroemer, H. Heterostructure bipolar transistors and integrated circuits. *Proc. IEEE* **70,** 13–25 (1982).

25. Chiang, C., Xu, C., Han, Z. & Ho, W. Real-space imaging of molecular structure and chemical bonding by single-molecule inelastic tunneling probe. *Science* **344,** 885–8 (2014).

26. Giannozzi, P. *et al.* QUANTUM ESPRESSO: a modular and open-source software project for quantum simulations of materials. *J. Phys. Condens. Matter* **21,** 395502 (2009).

27. Troullier, N. & Martins, J. L. Efficient pseudopotentials for plane-wave calculations. *Phys. Rev. B* **43,** 1993–2006 (1991).

28. Yang, L. et al. Quasiparticle energies and band gaps in graphene nanoribbons . *Phys. Rev. Lett.* **99**, 186801 (2007).

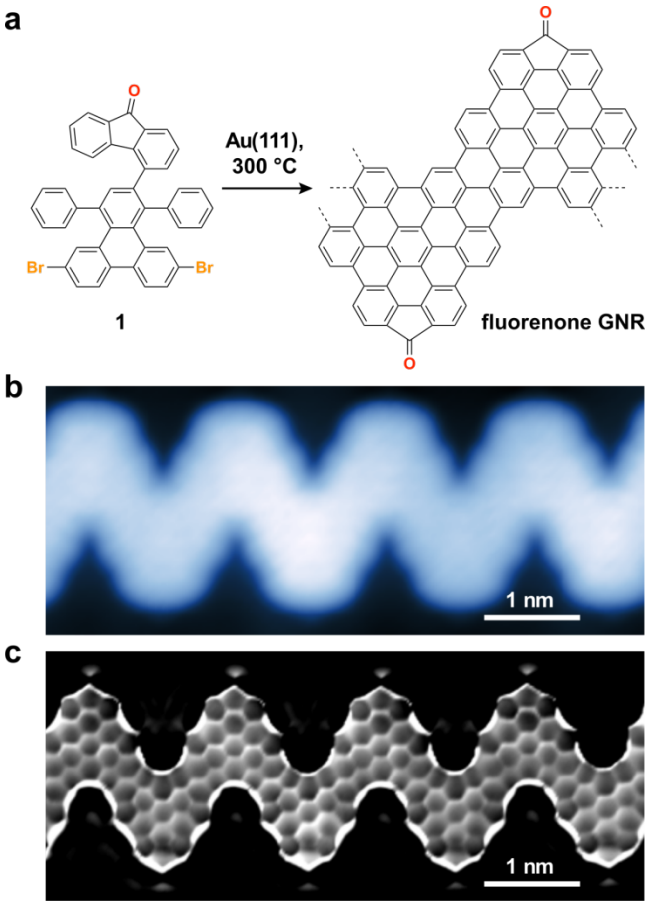

Figure 1 | Bottom-up fabrication of fluorenone GNRs. a, Schematic representation of the synthesis of fluorenone GNRs from molecular precursor **1**. **b**, Representative STM topographic image of a fluorenone GNR (CO functionalized tip, $V_s = -1.0$ V, $I_t = 10$ pA). **c**, BRSTM image of the same fluorenone GNR as in **b**. The covalent bond network within the GNR is clearly resolved ($V_s = 40$ mV, $I_t = 10$ pA, $V_{ac} = 20$ mV, $f = 401$ Hz).

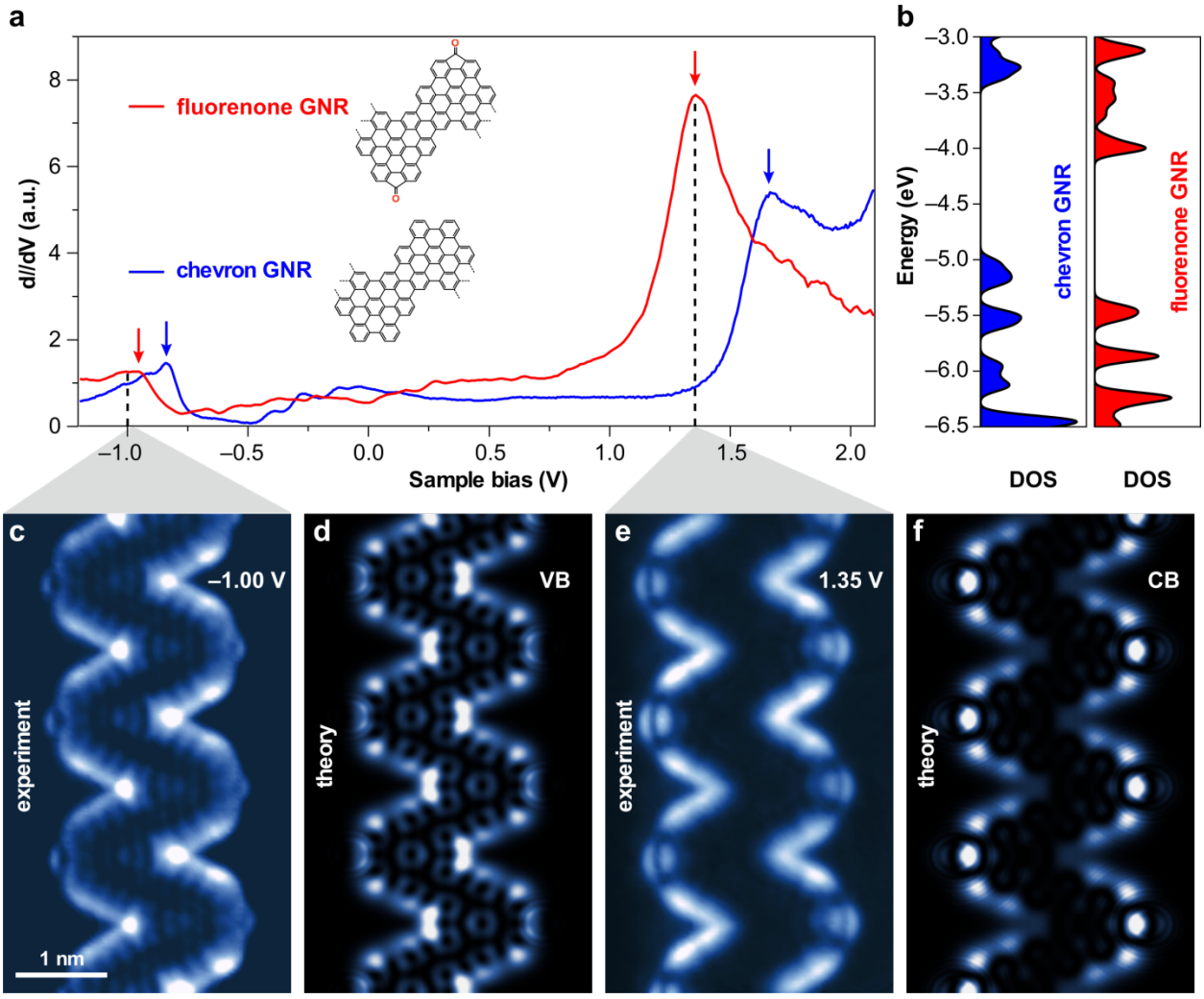

Figure 2 | Electronic structure of fluorenone and unfunctionalized chevron GNRs. a, STM d*I*/d*V* point spectra acquired for a fluorenone GNR (red) and an unfunctionalized chevron GNR (blue) on a Au(111) substrate (V_{ac} = 10 mV, f = 401 Hz, T = 4.5 K). **b,** Theoretical DOS calculated for isolated fluorenone GNR (red) and isolated unfunctionalized chevron GNR (blue) (energy is calibrated to the vacuum potential for both plots). **c,** Experimental d*I*/d*V* map of states at VB edge for a fluorenone GNR. **d,** Theoretical LDOS map of states at VB edge for a fluorenone GNR. **e,** Experimental d*I*/d*V* map of states at CB edge for a fluorenone GNR. **f,**

Theoretical LDOS map of states at CB edge for a fluorenone GNR. Experimental parameters for dI/dV maps: V_{ac} = 20 mV, f = 401 Hz, T = 4.5 K.

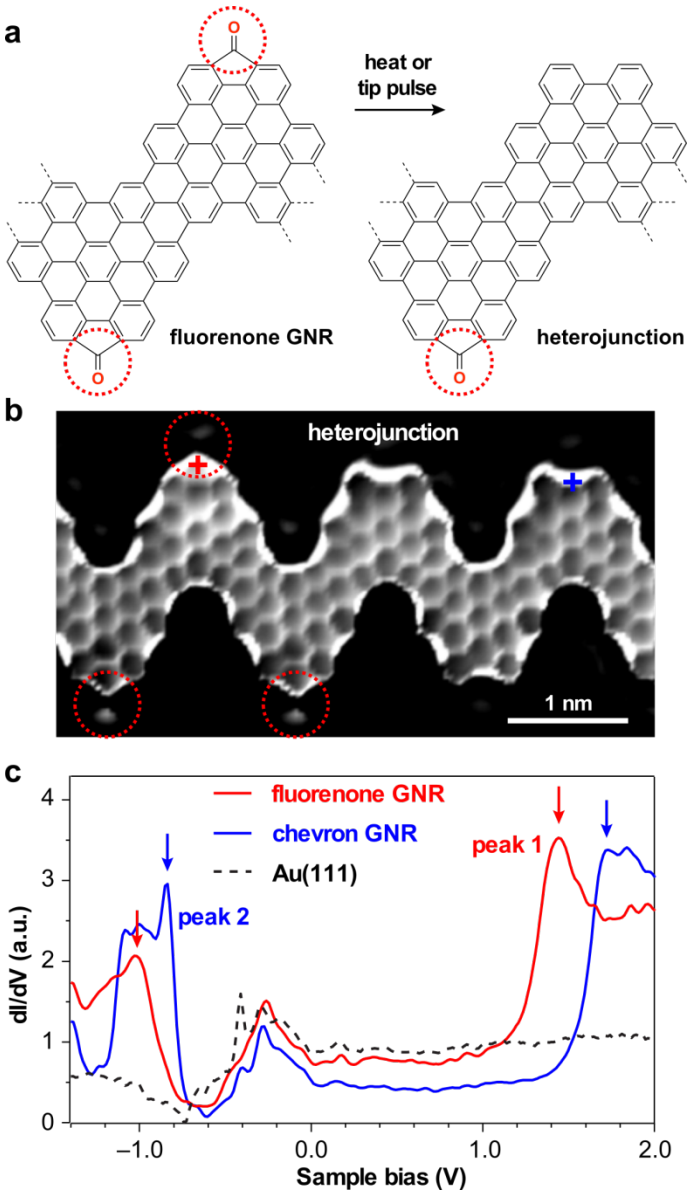

Figure 3: Electronic structure of fluorenone/unfunctionalized chevron GNR heterojunction. **a,** Schematic representation of the fabrication of a fluorenone/unfunctionalized chevron GNR heterojunction from a uniform fluorenone GNR. **b,** A BRSTM image of a fluorenone/unfunctionalized chevron heterojunction (V_s = 40 mV, I_t = 10 pA, V_{ac} = 20 mV, f = 401 Hz). Red dashed circles indicate the positions of fluorenone carbonyl groups. **c,** STM dI/dV

point spectra of the fluorenone/unfunctionalized chevron GNR heterojunction shown in **b** taken on both sides of the interface (crosses indicate the position where spectra were recorded in **b**).

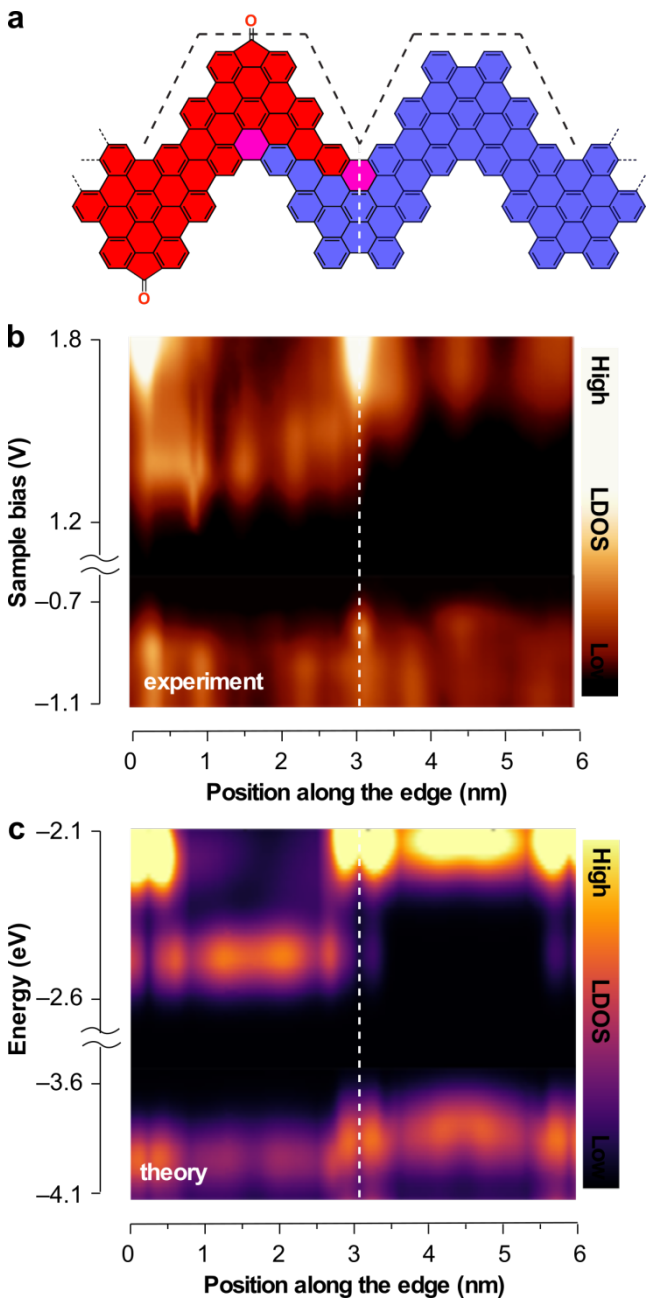

Figure 4 | Comparison of experimental and theoretical band edge alignment across the fluorenone/unfunctionalized chevron GNR heterojunction interface. a, Sketch of flourenone/unfunctionalized heterojunction shows tip trajectory. **b**, d*I*/d*V* spectra recorded along the edge of a heterojunction interface (back dashed line in **a**). Band bending of ~0.3 eV occurs over a distance of only ~0.6 nm across the fluorenone/unfunctionalized chevron GNR interface leading to an effective electric field of 5 x 10^8 V m^{-1}. **c**, Theoretical calculation of the local density of states (LDOS) energy dependence along the edge of a fluorenone/unfunctionalized chevron GNR heterojunction as shown in **a** (LDOS was averaged at each point over a 4 Å radius and Gaussian broadening of 0.1 eV was used; the intensity of the valence band structure was increased by a factor 3 for better resolution of the energy gap).

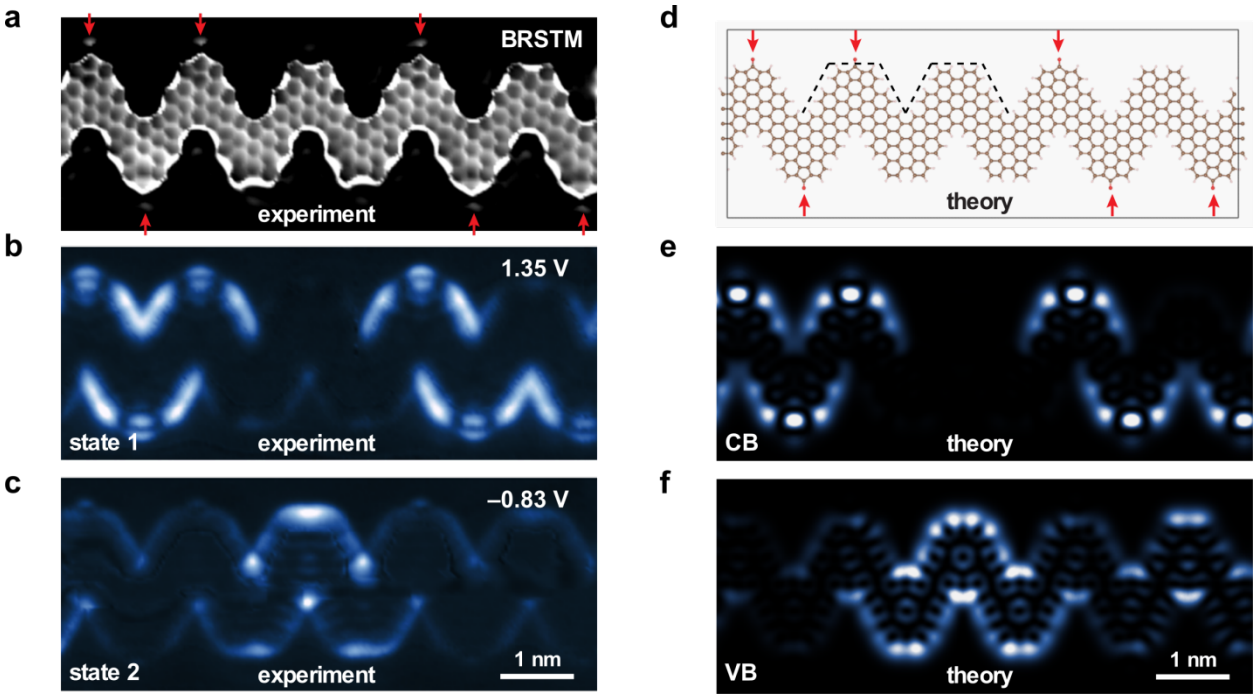

Figure 5 | Comparison of experimental *dI/dV* maps and theoretical LDOS for a fluorenone/unfunctionalized chevron GNR heterojunction. a, BRSTM image of a GNR exhibiting two fluorenone/unfunctionalized chevron GNR heterojunctions surrounding a central

unfunctionalized chevron GNR segment (V_s = 40 mV, I_t = 10 pA, V_{ac} = 20 mV, f = 401 Hz). Red arrows indicate the positions of carbonyl groups. **b,** Experimental STM dI/dV map of fluorenone/unfunctionalized chevron GNR heterojunctions recorded at CB edge energy = +1.35 V (peak 1 in Fig. 3c) and **c,** dI/dV map of fluorenone/unfunctionalized chevron GNR heterojunctions recorded at VB edge energy = −0.83 V (peak 2 in Fig. 3c) (V_{ac} = 20 mV, f = 401 Hz). **d,** Unit cell used to simulate LDOS of heterojunction system depicted in **a**. Black dashed line shows heterojunction interface along trajectory used to calculate gap dependence shown in Fig.4c. **e,** Calculated LDOS map 4 Å above GNR for states at CB edge of heterojunction structure shown in **d**. **f,** Calculated LDOS map 4 Å above GNR for states at VB edge state of heterojunction structure shown in **d**.